Catalysis Science & Technology

Accepted Manuscript

ROYAL SOCIETY OF CHEMISTRY

www.rsc.org/catalysis

Table of Contents

A highly active and recyclable Mn-doping ceria heterogeneous catalyst ($MnOx\text{-}CeO_2$) has been developed for the synthesis of aliphatic carbamates from CO_2, aliphatic amines and methanol in one step.

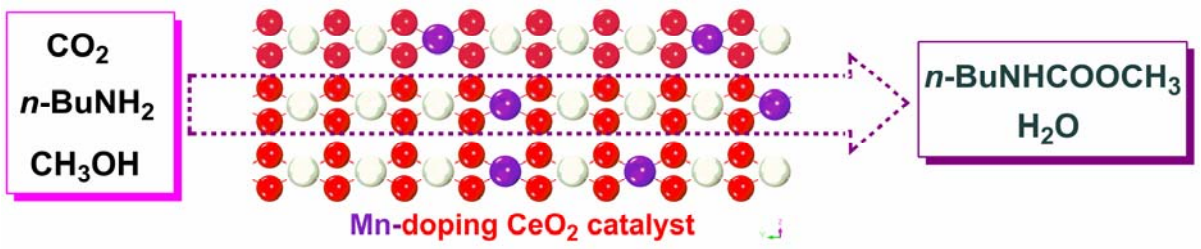

The Role of Mn doping in CeO_2 for Catalytic Synthesis of Aliphatic Carbamate from CO_2

Ran Zhang, Li Guo, Chen Chen, Jizhong Chen, Angjun Chen, Xiuge Zhao, Xuerui Liu, Yuhe Xiu, Zhenshan Hou*

Key Laboratory for Advanced Materials, Research Institute of Industrial Catalysis, East China University of Science and Technology, Shanghai, 200237, China.

Tel: +86 21 64251686, Fax: +86 21 64253372

E-mail: houzhenshan@ecust.edu.cn

Abstract: A novel highly active Mn-doping ceria heterogeneous catalyst (MnO_x-CeO_2) was prepared and dedicated to the catalytic synthesis of aliphatic carbamates from CO_2, aliphatic amines and methanol in one step. The as-obtained catalyst can attain high yield of carbamate up to 82%, and can also be recycled at least for four times through simple procedure. It was observed that the Mn doping to ceria can alleviate the catalyst deactivation in the consecutive catalytic recycles. In this regards, the role of Mn doping in the ceria in the synthesis of the aliphatic carbamates was investigated by means of X-ray diffraction (XRD), Raman spectra, specific surface areas (BET), thermogravimetric analysis (TGA), X-ray photoelectron spectroscopy (XPS), CO_2-Temperature programmed desorption (CO_2-TPD) and *in-situ* diffuse reflectance infrared Fourier transform (DRIFT). The characterization demonstrated that the presence of MnO_x in the ceria can not only inhibit the formation of stable carbonate species on the surface of the catalyst but also promote the decomposition/consuming of the carbonaceous species during the synthesis of aliphatic carbamates so as to allow improving the recyclability of catalyst.

Keywords: Ceria; Manganese oxide; Carbon dioxide; Amines; Carbamates

Introduction

Organic carbamates have very important applications in chemistry, such as the functional group of polyurethanes in polymer chemistry, protective groups of amines in peptide or related chemistry, and as active ingredients of insecticides in agricultural chemistry.[1] The as-prepared carbamates can also be used as organic solvents as well as organic intermediates for polyurethane to manufacture plastics, rubbers, fibers, rigid and soft foamed plastics, adhesives, coatings, etc.[2] Conventional synthesis routes to prepare carbamates mainly involve alcoholysis and aminolysis using highly toxic phosgene as a raw material.[3] In addition, in recent years, environmental issues have resulted in increasing attention.[4] Many countries take initiatives in seeking novel synthesis processes to gradually replace the methods using toxic phosgene, such as reductive carbonylation of nitro aromatics,[5] oxidative carbonylation of amines,[6] alcoholysis of urea derivatives[7] and carboxylation of amines.[8] However, the routes will suffer from a lack of economical viability in the near future or hazards in handling of carbon monoxide and oxygen under high pressures.

On the other hand, the rise in carbon dioxide levels in the global environment has led to an increased desire to fix and comprehensively use carbon dioxide as a potential carbon resource, while ensuring energy conservation and emission reduction.[9] As carbon dioxide is stable, non-toxic, non-corrosive, flame-retardant and easily processed, it is one of the most widely distributed, most abundant in storage and cheapest carbon resource.[10] Therefore, it has always been one of the most focused issuses on green chemistry that CO_2 is employed to replace the limited and non-renewable petrochemical resources by C_1 synthetic reaction, and prepare useful compounds by various chemical conversions, which has both important application values and theoretical research significance.[11] Thus methods for synthesizing organic carbamates in one step using carbon dioxide, organic amine and alcohol as raw materials have drawn particular interest.[12] However, the drawback of these catalytic systems lies in the need of a large amount of expensive dehydrant; the relatively rigorous reaction condition (30 MPa CO_2, 200 ^{o}C, 24 h), or suffer from not being

recycled.[13] Recently, Tomishige's research group employed commercialized CeO_2 as a heterogeneous catalyst to synthesize a carbamate in one step from carbon dioxide, benzylamine and methanol.[14] However, the catalyst afforded poor activity for the conversion of aliphatic amines and also needed to be calcined at higher temperature after reaction for the next run. Because aliphatic amines are cheaper and less toxic than aromatic amines, the synthesis of carbamates from aliphatic amines and carbon dioxide over a reusable, highly active catalyst would be a more promising approach in producing carbamates.

Continuing our previous work on CO_2 utilization,[15] we attempted to synthesize carbamate from CO_2, amine and CH_3OH using a heterogeneous catalyst in this work. Herein, a highly active Mn-doping ceria heterogeneous catalyst (MnO_x-CeO_2) has been developed and was dedicated to converting aliphatic amines, methanol and carbon dioxide into carbamates in one step by a catalytic approach. To identify the reason for deactivation of CeO_2 catalyst and the role of MnO_x in the MnO_x-CeO_2 catalyst, a systematic study of synthesis of N-butylcarbamate from n-butylamine, CO_2 and methanol was performed to understand reaction intermediates on the catalyst surface of ceria and Mn-doping ceria catalysts, as well as the role of MnO_x in the MnO_x-CeO_2 on improving the stability of the catalyst.

Experimental

Materials

All chemicals were analytical grade and commercially available. They were used without further purification, unless otherwise stated. N-butylamine (BA, ⩾98.5%), was obtained from Lingfeng Chemical Reagent Co., Ltd., Shanghai. CO_2 (>99.95%) and N_2 (>99.999%) were supplied by Shanghai Shangnong Gas Factory. The commercialized CeO_2 (denoted as CeO_2-com) was purchased from Aladdin (nanopowder, 20-50 nm beads with purity of 99.9 %) and calcined at 600 ^oC for 3 h prior to use. All the other materials were obtained from SCRC (Sinopharm Chemical Reagent Co., Ltd., Shanghai).

Catalyst preparation

The mixed oxides MO_x-CeO_2 (M=Mn, Ca, Ba, Ti, In, Fe, Sn, Co, Zn, or Al), were prepared by co-precipitation method. A certain amount of metal (M) nitrate was weighed and dissolved in pure water to ensure the content of the metal in the solution to be 1.0 mg/ml. Then the pre-weighed $Ce(NO_3)_3 \cdot 6H_2O$ solid was poured into the above formulated nitrate solution. The mixture was sonicated to obtain a homogeneous solution. A solution of $NH_3 \cdot H_2O$ (1:10) was added dropwise to the reaction system under vigorous stirring to adjust the pH value of the solution to 9.5. The solution was continuously stirred for another 4 h after the addition of aqueous ammonia, and a large amount of solid was filtered, washed with water to neutrality, and dried in a drying oven at 80 ^oC overnight. The as-prepared solid catalyst was then calcined in a Muffle furnace at 600 ^oC for 3 h. The final products were denoted as MO_x (X)-CeO_2, where X represented a molar fraction of M in Ce and M, i.e. X=M/(Ce + M). Similarly, laboratory-made CeO_2 (X=0) and Mn_2O_3 (X=1) catalysts have also been prepared, which were denoted as Lab-CeO_2 and Mn_2O_3, respectively.

Catalyst characterization

All catalysts were characterized by XRD which was carried out on a Rigaku D/max 2550VB/PC X-ray diffractometer (with a variable slit width). Graphite monochromator, Cu-Kα target (λ＝0.15056 nm), tube voltage 40 kV, tube current 40 mA, emission slit (1/6)°, scan rate 6 (^{o})/min, scan area 10-80^o. The BET areas of the catalysts were measured by the N_2 adsorption-desorption method at liquid nitrogen temperature using a Quantachrome Instrument. The catalysts were pre-treated at 200 °C for 12 h under vacuum before the test. The Raman spectra were recorded for solids on an inVia Raman microscope using the exciting wavelength from a laser at 514 nm. Scanning electron microscopy (SEM) image and energy dispersion spectrum (EDS) mapping were performed on HITACHI S-3400N equipped with an EDS APPOLLO X. The TGA patterns of catalysts were performed with using a Perkin-Elmer Diamond TG/DTA 6300 instrument. The catalysts were heated up to 800 ^oC at a constant rate of 20 $^oC \cdot min^{-1}$ under N_2 atmosphere. XPS measurements were measured using a

Thermo ESCALAB 250 X-ray photoelectron spectrometer, using Al Kα as the excitation sources. All binding energies were referenced to the C1s peak at 284.8 eV for adventitious carbon. XPS data were analyzed using XPS peaking software. All peaks of the corrected plot were fitted with a Gaussian–Lorentzian shape function to peak fit overlapping features. Iterations were performed using the Marquardt method. Standard deviations were always lower than 1.5%.

Temperature-programmed desorption (TPD) of CO_2 was carried out in a flow system to observe basic properties of the catalysts. Prior to CO_2-TPD experiments, the samples (100 mg) were first reduced at 500 ^oC for 1 h under H_2 flow and then oxidized at 400 ^oC for 1 h under 5 % O_2 (He) flow to remove the residual water or carbonates. The samples were then cooled to room temperature and CO_2 adsorption was performed by flowing this gas through the samples for 30 min, followed by He flow for 30 min at room temperature to eliminate physically adsorbed CO_2. Subsequently, desorption was carried out from 30 ^oC to 500 ^oC at a heating rate of 10 $^oC \cdot min^{-1}$ under flowing He and kept at that temperature for 10 min. The desorbed CO_2 was quantified using a thermal conductivity detector (TCD). Calibration was performed using pulses of CO_2.

DRIFT spectra were recorded with a NICOLET 6700 spectrometer (Thermo Scientific) equipped with a liquid nitrogen-cooled MCT (HgCdTe) detector (resolution 4 cm^{-1}). An *in-situ* cell capable of high temperature gas flow operation and fitted with ZnSe windows served as the reaction chamber for *in-situ* adsorption and reaction measurements. The spectra of adsorbed *n*-butylamine (BA), CO_2 and methanol was recorded in the following method: about 30 mg catalyst was mounted into the ceramic pan in *in-situ* IR cell and pretreated in He flow (48 ml · min^{-1}) at 500 ^oC for 1 h, prior to cooling to 30 ^oC. Then, BA was introduced by He flow while the temperature was kept at 30 and 170 ^oC, respectively. Next, the pipelines were purged for 30 min by He flow to remove the residual BA and then CO_2 stream (48 ml·min^{-1}) was introduced while the temperature was kept at 170 ^oC. All the spectra were recorded after BA or CO_2 was introduced for 5 min. Next, CH_3OH was injected under the CO_2 stream, which was fed to the *in-situ* IR cell. The spectra of co-adsorbed BA,

methanol and CO_2 were measured. After 1.5 h, the loaded catalyst was purged with He flow (37 ml · min^{-1}) and the spectra were recorded at 300 and 500 ^oC, respectively. All spectra were obtained by subtraction of spectrum derived from air and the apparatus.

Reaction Procedure

All the reactions were carried out in 50 ml of autoclave reactor with PTFE liner (working capacity of approximately 40 ml). A typical procedure for the linear carbamate synthesis from BA, methanol, and CO_2 was described as follows: 0.3 g of MnO_x-CeO_2 catalyst, BA (5 mmol) and methanol (500 mmol) were put into the reactor together with a stirring bar, and then the reactor was purged with CO_2. After that, CO_2 was injected by a high-pressure pump (the reaction pressure was 5 MPa). The reactor was heated to reaction temperature with continuously stirring by a magnetic stirrer. After the reaction time, the reactor was cooled in an ice-water bath. CO_2 was released slowly by passing it through a cold trap containing methanol to absorb trace amounts of reactant and product entrained in the CO_2 stream. The reaction solution was separated from the solid catalyst by simple centrifugation and toluene was added to the liquid phase as an internal standard for a quantitative analysis. The collected liquid phase was analyzed by GC analyses (Shimadzu GC-2014 apparatus equipped with a KB-50 column and FID detector) and GC-MS analyses (Agilent-6890/GC-5973MS with a HP-5 column) to obtain the conversion of BA and the selectivity to N-butylcarbamate (NBCB) and N,N-dibutylurea (DBU) ($Sel._{NBCB}$ and $Sel._{DBU}$), while the reactant and product moles (n_{BA}, n_{NBCB}, n_{DBU} and n_{DMC}) after reaction were also obtained from the relative sensitivity, respectively (Table S1).

For the recycling of catalyst, after reaction the catalyst was washed with methanol for three times to remove the residual substrates and the organic products adhered to the catalyst surface. The washed catalyst was dried in drying oven at 110 ^oC overnight for the regeneration of the catalyst. The regenerated catalyst could be reused directly, where all the reaction condition and operation procedure should be

consistent with the last run.

Results and Discussion

Considering the effect of different metal oxides in general, and thus an appropriate promoter for CeO_2 catalyst was chosen in the direct synthesis of N-butylcarbamate (NBCB) from BA, methanol and CO_2, M-doping ceria catalysts MO_x-CeO_2 (M=metals) were prepared by a conventional co-precipitation method. Herewith, we prepared various ceria catalysts doped with various metals, including Mn, Ca, Ba, Ti, In, Fe, Sn, Co, Zn, or Al. The reaction equation for synthesizing NBCB over different CeO_2-based catalysts from BA, CO_2 and methanol is shown in Scheme 1. Moreover, dibutylurea (DBU) and dimethyl carbonate (DMC) were detected as minor by-products in the synthetic reaction.

<Insert scheme 1 here>

Catalytic activity

Figure 1 showed the BA conversion and selectivity to NBCB over CeO_2-com and Lab-CeO_2 catalysts, as well as the M-doped ceria catalysts MO_x-CeO_2 (M=Ca, Ba, Ti, In, Fe, Sn, Co, Zn, Mn, or Al). It can be seen that the conversion and selectivity over Lab-CeO_2 catalyst was much higher than that of the CeO_2-com catalyst. In addition, among all M-doped ceria catalysts, the Al_2O_3(0.03)-CeO_2 and MnO_x(0.03)-CeO_2 catalysts showed higher conversion and selectivity, in comparison with other CeO_2-based catalysts. Regarding such a finding, the effect of the composition of (Al_2O_3(X)-CeO_2 and MnO_x(X)-CeO_2) catalysts on the conversion of BA and selectivity was sequentially examined and results were shown in Figure 2. As seen in Figure 2a, the Al_2O_3(X)-CeO_2 catalysts with higher Al content (X > 0.03) tended to decline both conversion and selectivity, while the catalyst with lower Al content (X < 0.03) showed similar activity with the Lab-CeO_2 catalyst. Interestingly, MnO_x(X)-CeO_2 catalyst exhibited a very similar tendency for catalytic performance as that of Al_2O_3(X)-CeO_2 catalysts, where the highest conversion also appeared at

X=0.03 (Figure 2b). However, it should be noted that the selectivity could remain unchanged in a more wide range of X from 0.1 to 0.01 over the MnO_x(X)-CeO_2 catalyst, compared with Al_2O_3(X)-CeO_2 ones. Hence, the following research will be focused on the Lab-CeO_2-and MnO_x(0.03)-CeO_2 catalysts.

<Insert Figure 1 here>

<Insert Figure 2 here>

Firstly, the BA conversion and selectivity to NBCB and DBU versus time profile over Lab-CeO_2 and MnO_x(0.03)-CeO_2 catalysts was plotted in Figure 3. For the Lab-CeO_2 catalyst, the conversion increased smoothly with the reaction time at the beginning of reaction and then reached a maximum of 84.7% after 8 h, but the conversion showed slight decrease in the prolonging time likely due to the reversible reaction (Figure 3A). It was worth noting that the selectivity to NBCB declined normally along with increase of the selectivity to DBU simultaneously over the Lab-CeO_2 catalyst (Figure 3B). On the other hands, the BA conversion over the MnO_x(0.03)-CeO_2 catalyst achieved 86.5% at 8 h and showed a little increase with the longer reaction time (16 h) (Figure 3C). Meanwhile, the selectivity to NBCB over MnO_x(0.03)-CeO_2 catalyst remained almost unchanged during the initial 8 hours and only showed a little decrease after 10 h accompanied by the rising of the selectivity to DBU (Figure 3D). DMC was detected as a minor species during the reaction over the two catalysts (Figure S1). On the basis of the results above, it was indicated that both DMC and DBU were possible intermediates for the synthesis of NBCB from BA and CO_2 as starting materials (Scheme 2).

<Please insert Figure 3 here>

<Please insert Scheme 2 here>

The effect of pressure on the catalytic reaction was illustrated in Figure S2. The conversion of BA kept almost unchanged above 5 MPa, while the $Sel._{NBCB}$ showed gradual decrease with increasing pressure, which might result from inhibiting alcoholysis of DBU due to excess of CO_2. In addition, the other reaction conditions, such as temperature, the ratio of substrate to catalyst, and BA to CH_3OH ratio, were all examined and shown in Figure S3, Table S2 and Table S3.

Then the Lab-CeO_2, Al_2O_3(0.03)-CeO_2 and MnO_x(0.03)-CeO_2 catalysts were subjected to recycling and the results were shown in Figure 4. It was worth noting that the selectivity to NBCB was substantially increased when more CH_3OH was added over the three catalysts. The catalytic activity of fresh MnO_x(0.03)-CeO_2 and Al_2O_3(0.03)-CeO_2 catalyst was as good as that of the fresh Lab-CeO_2 catalyst at 8 h. Most importantly, it can be observed that both Lab-CeO_2 and Al_2O_3 (0.03)-CeO_2 catalysts deactivated quickly upon reuse. In contrast, the catalyst MnO_x (0.03)-CeO_2 showed much higher catalytic stability and can be reused at least four recycles with no loss of activity and only a slight decrease of selectivity to NBCB. In addition, for the three catalysts, it was worth noting that the decrease in selectivity to NBCB always accompanied by the increase of selectivity to DBU after four recycles. It is thus clear that the existence of MnO_x in MnO_x(0.03)-CeO_2 catalyst played a remarkable role in improving the stability of the catalyst. Herein, a systematic investigation was carried out to identify the possible influence of Mn doping on ceria structure and thus to understand the role of MnO_x in improving the catalytic stability by a series of characterization techniques.

<Insert Figure 4 here>

Catalyst structure

Wide angle XRD patterns of Lab-CeO_2, Mn_2O_3(X=1), and MnO_x(0.03)-CeO_2 catalysts are shown in Figure 5. As shown in Figure 5a, the intensive and sharp diffractions at 2θ = 23.1 °, 32.9 °, 38.2 °, 45.2 °, 49.3 °, 55.2 ° and 65.8 ° proved the presence of pure Mn_2O_3 phase (JCPDS No. 89-4836/65-1798).[16] The main reflections at 2θ=28.5, 33.1, 47.5, 56.4, 59.1, 69.3, and 76.7° over Lab-CeO_2, CeO_2-com and MnO_x(0.03)-CeO_2 are indexed well to the typical cubic fluorite-like structure of CeO_2 (JCPDS No. 81-0792).[17] A more asymmetric shape of such reflections with lower intensity confirms the weakening degree of the crystallinity of the MnO_x(0.03)-CeO_2 catalyst when compared to pure Lab-CeO_2, which was consistent with the increase in surface area (Table S4). The corresponding crystallite size for the Lab-CeO_2 and CeO_2-com was calculated from the (111) plane of ceria using Scherrer equation,[18]

which was 14 nm and 37 nm, respectively. Interestingly, the calculated size of $MnO_x(0.03)$-CeO_2 particle is only 7 nm. In addition, the TEM images showed that the average particle size of $MnO_x(0.03)$-CeO_2 catalyst (9 nm) is much smaller than that of parent Lab-CeO_2 (15 nm) (Figure 6A and 6C). TEM images actually reveal a broad particle distribution (12-20 nm for the Lab-CeO_2 catalyst and 8-12 nm for the $MnO_x(0.03)$-CeO_2 catalyst). These results are in agreement with the values obtained by the XRD characterization.

<Please insert Figure 5 here>

<Please insert Figure 6 here>

In the next step, a subtle cubic lattice distortion due to Mn-doping was proved by Raman spectroscopic data (Figure 7). The small peak centered at 633 cm^{-1} can be ascribed to the Mn–O stretching mode arisen from the Mn_2O_3 species (Figure 7a).[19] The main band centred at 463 cm^{-1} is typical of CeO_2 vibrations due to the triply degenerated TO mode (Figure 7b).[20] However, there was no observable band of MnO_x in the spectrum of the fresh $MnO_x(0.03)$-CeO_2 catalyst and the Raman peak arisen from CeO_2 vibrations shifted to lower wavenumber occurring at about 447 cm^{-1} (Figure 7c), which could be attributed to the diffusion of partial Mn species into the fluorite lattice, resulting in aberration of CeO_2 structure. The Raman peaks are related to the physical-chemical structure of the catalysts. The full width at half maximum (FWHM) has been related to the crystallite size and/or the amount of oxygen vacancies.[21] The FWHM value in the case of $MnO_x(0.03)$-CeO_2 (FWHM = 44 cm^{-1}) was much larger than that of Lab-CeO_2 (FWHM = 14 cm^{-1}), suggesting that $MnO_x(0.03)$-CeO_2 showed smaller crystallite size, which was in well agreement with that of XRD and the TEM analysis (Figure 5 and Figure 6). In addition, the SEM EDS mapping of the $MnO_x(0.03)$-CeO_2 catalyst showed the uniform distribution of the doped Mn (Figure 8).

<Please insert Figure 7 here>

<Please insert Figure 8 here>

As described above all, the Lab-CeO_2 catalyst by precipitation method with lower average particle size (14 nm) showed higher catalytic activity than that of the

CeO_2-com catalyst with large particle size (37 nm), which was in agreement with the fact that a large surface area is beneficial for the catalytic activity of CeO_2 nanoparticles (Table S4), as shown in the previous report.[22] Nevertheless, the Lab-CeO_2 catalyst still showed poor recyclability (Figure 4). On the other hand, doping of MnO_x into ceria by co-precipitation not only resulted in much smaller particle size of the catalyst (MnO_x(0.03)-CeO_2, 7 nm), indicating comparable catalytic activity with the Lab-CeO_2 catalyst, but also largely promoted the recyclability of the catalyst (Figure 4). In addition, the results of CO_2-TPD showed that Mn doping in ceria contributed to lowering the surface basicity of the ceria catalyst and thus weakened interaction of surface with CO_2 (Figure S4), which was consistent with previous report.[23] Then, the following work will be focused on investigating the role of MnO_x doping in improving the stability of the catalyst.

Deactivation mechanism of the ceria catalysts

It has been reported that the catalyst deactivation still remained problematic for the efficient synthesis of aromatic carbamates or cyclic ureas from CO_2 over ceria catalyst.[14,22] Even if the catalyst was regenerated by calcination, the activity can still not be fully recovered. The deactivation mechanism of ceria for the synthesis of linear carbamate has still remained not very clear. In this work, the catalytic stability of Lab-CeO_2 and MnO_x(0.03)-CeO_2 catalysts was examined in the synthesis of NBCB and thus deactivation mechanism of ceria-based was discussed accordingly.

The mechanism was firstly identified according to the reaction route (A). As shown in Table 1, the Lab-CeO_2 catalyst deactivated completely after three recycles when subjecting to carbonylation reaction of BA with CO_2 into DBU (Table 1, entries 1-3). However, the MnO_x(0.03)-CeO_2 catalyst showed excellent catalytic stability in the recycles. Next, the alcoholysis of DBU with methanol into NBCB over the Lab-CeO_2 and MnO_x(0.03)-CeO_2 catalysts was also examined (Table 2), respectively. The Lab-CeO_2 catalyst can be reused twice without activity loss under N_2 atmosphere (Table 2, entries 2-3). In addition, no DMC was detected suggesting that alcoholysis reaction of DBU to DMC cannot happen under the present condition. However, when

the reaction was conducted over Lab-CeO_2 catalyst under CO_2 atmosphere, the n_{NBCB} was increased to 2.7 mmol and the n_{BA} was reduced to 0.5 mmol, which was not consistent to the stoichiometric ratio of the reaction equation (Table 2, entry 4). We can infer that the forming BA continued on reacting with CO_2 to produce DBU and then resulted in more NBCB formation through the cascade reaction. After three consecutive recycles in CO_2 atmosphere, both alcoholysis reaction of DBU and carbonylation of amine were inhibited (Table 2, entries 4 and 5) although the activity can be almost recovered when the spent catalyst was calcined in O_2 at 220 ^oC for 2 h (Table 2, entry 6). On the other hand, the alcoholysis reaction of DBU over the MnO_x (0.03)-CeO_2 show much higher activity than Lab-CeO_2 catalyst (n_{NBCB}=3.8 mmol) and proceeded very smoothly for three consecutive recycles without significant deactivation (Table 2, entries 7-9). In the view of the results above, it was suggested that CO_2-derivative species adsorbed on the Lab-CeO_2 catalyst surface during the reaction and poisoned the catalyst, which can be removed by calcinations in O_2 atmosphere to restore the activity of catalyst. In contrast, the Mn-doping ceria catalyst seemed to resist significantly on poisoning by CO_2-derivative species and then showed excellent recycability in alcoholysis reaction of DBU even in the presence of CO_2.

<Please insert Table 1 here>

<Please insert Table 2 here>

In the next step, the reaction of methanol with CO_2 was conducted over Lab-CeO_2 and MnO_x (0.03)-CeO_2 catalysts and only trace amount of DMC was formed (Table S5), suggesting that the reaction of methanol and CO_2 to form DMC is not favorable under the present condition due to thermodynamic limit. On the other hand, as shown in Table S6, the carbonylation of amine with DMC afforded low activity although NBCB was detected as the main product over MnO_x(0.03)-CeO_2 catalyst under N_2 atmosphere. However, the reaction activity increased but main product was DBU under CO_2 atmosphere mainly due to the carbonylation of BA by CO_2 to produce DBU under the reaction condition. This indicated that the direct carbonylation of amine with CO_2 into DBU can proceed easily under the present

reaction conditions over CeO_2 and $MnO_x(0.03)$-CeO_2 catalysts, as also was confirmed by the previous results (Table 1, entry 1 and 4). Hence, the reaction route (A) in Scheme 2 contributes more than the reaction route (B) during the reaction.

As demonstrated by the various characterization including the XRD, Raman, TEM, BET, TG, XPS and DRIFT techniques, the deactivation mechanism and the promotion role of MnO_x in the ceria were discussed in the following. No phase transformations were observed in their XRD patterns (Figure 5), although TEM characterization showed that the slight aggregation of the particle happened after reaction (Figure 6). Meanwhile, the specific surface area of the spent Lab-CeO_2 and MnO_x (0.03)-CeO_2 catalyst did not decline obviously (Table S4). However, the TG analysis showed that the obvious weight loss occurred at a wide range of 100-1000 ^oC especially in range of 400-800 ^oC over the spent Lab-CeO_2 catalyst, whereas was not seen over the spent $MnO_x(0.03)$-CeO_2 catalyst (Figure 9). It can be preliminary deduced that some stable substances were deposited on the catalyst surface and thus difficult to decompose, resulting in poisoning the catalyst.

<Please insert Figure 9 here>

Then XPS spectra of Ce 3d (A), O 1s (B) and C 1s (C) of the fresh and spent catalysts (Lab-CeO_2 and $MnO_x(0.03)$-CeO_2) were conducted (Figure 10), and the data were summarized in Table S6. The Ce 3d Gaussian peak fits corresponding to Ce^{3+} and Ce^{4+} states are based on published CeO_2 XPS analysis by Larachi et al.[24] Typically, the Ce 3d XPS core-level spectra exhibited three-lobed envelopes (around 879–892 eV, 892–910 eV and approximately 916 eV) for both the fresh Lab-CeO_2 and $MnO_x(0.03)$-CeO_2 catalysts (lines a and c in Figure 10A).[25] Since the general line width varied significantly with the amount of surface charging as revealed by the width of the u''' satellite feature and Ce^{3+} compounds do not exhibit the u''' satellite, the present discussion of Ce^{4+} reduction will be focused on the contribution of this feature to the total Ce 3d intensity which decreases with increasing reduction degree of ceria.[26] As shown in Table S6 (entries 1 and 3), the value of u'''/total area showed no significant difference between the fresh Lab-CeO_2 and $MnO_x(0.03)$-CeO_2 catalysts, revealing that the reduction degree of ceria kept nearly unchanged, that is, the

concentration of oxygen vacancies was basically the same.

<Please insert Figure 10 here>

As shown in Figure 10B (lines a and c), O 1s spectrum of fresh Lab-CeO_2 has a broad peak at 526.5-530 eV, assigned to lattice oxygen (O_L). Two shoulder peaks at ca. 531.1 and 532.3 eV are observed, which can be attributed to adsorbed oxygen and weakly bonded oxygen species i.e. active oxygen (O_s), and to surface oxygen by hydroxyl species and adsorbed water species as contaminants at the surface (O_a), respectively.[27] It was observed that O 1s core level of lattice oxygen on MnO_x (0.03)-CeO_2 catalyst shifts to high values because of ''Mn←O'' electron-transfer processes.[28] In addition, there were three different carbon species on the catalytic surface: adventitious carbon (C_{adv}, 284.8 eV), O=C–H species (C_1, 287.2 eV), carbon associated with adsorbed CO_2 (C_2, 289.4 eV) (Figure 10C).[29] Deconvolution of the C 1s spectra indicated the surface of the fresh Lab-CeO_2 and MnO_x(0.03)-CeO_2 catalysts may have partially been contaminated by CO_2 in air (lines a and c in Figure 10C). For most of ceria catalysts, an atomic O/Ce ratio is <2, while the initial high oxygen level of both the Lab-CeO_2 and MnO_x(0.03)-CeO_2 catalysts is largely ascribed to by surface absorbed water, and CO_2-related contaminants (Table S7, entries 1 and 3).[30]

However, as shown in Figure 10, Ce 3d level of the spent Lab-CeO_2 catalyst shifted substantially to higher values and simultaneously the absorption spectrum with the O_L signal shifted from 528.7 eV to 529.1 eV showing a rise of the signal at 531.3 eV that is very weak in the fresh Lab-CeO_2 catalyst. Moreover, the new peaks at 288.9 eV (C_3, peak of –COOR: CO_3^{2-} species) and 291.3 eV (C_4, polydentate carbonate) increased significantly for the spent Lab-CeO_2 which testified further that new carbonaceous deposition occurred over the Lab-CeO_2 catalyst surface after subjecting to the reaction.[31] In contrast, the Ce 3d, O1s and C1s spectra of the spent MnO_x(0.03)-CeO_2 catalyst showed no significant change in comparison with the fresh catalyst, which revealed that the catalyst surface texture was relatively stable in this case. In addition, the Mn 2p spectrum of MnO_x(0.03)-CeO_2 confirmed the coexistence of three kinds of Mn species,[27] Mn^{2+}, Mn^{3+} and Mn^{4+} on the surface of MnO_x(0.03)-CeO_2 catalyst (Figure 10D). However, the Mn 2p spectra of XPS showed

weak signal due to very low Mn content in the catalyst so that it cannot give more accurate information of the difference in the oxidation state of Mn between fresh catalyst and the spent catalyst. These results were very strong evidence that large amount of CO_2-derived species deposited on the Lab-CeO_2 catalyst surface during the reaction from CO_2, BA and CH_3OH resulted in the reorganization of the surface structure, while the deposition of carbonaceous species became restricted over MnO_x(0.03)-CeO_2 catalyst.

In order to clarify further the deactivation mechanism and the promotional effect of MnO_x in the MnO_x(0.03)-CeO_2 catalyst, DRIFT of *in-situ* BA, CO_2 and CH_3OH adsorption was performed over Lab-CeO_2 and MnO_x(0.03)-CeO_2 catalysts (Figures 11-13). After BA was introduced into the Lab-CeO_2 catalyst at 170 ^oC, C-H stretching vibration (bands at 2965, 2936, and 2879 cm^{-1}) and N-H bending vibration (1626 cm^{-1}) of adsorbed BA were observed, which indicated that BA is coordinatively adsorbed to the Lewis acid sites on the catalyst surface (Figure 11a).[32] Next, Introduction of CO_2 to BA-adsorbed Lab-CeO_2 resulted in three main peaks 1651, 1525, 1292 cm^{-1}, and minor peaks 1669, 1606, 1324, and 1223 cm^{-1} under CO_2 flow, all these bands can be assigned to absorption of carbamic acid or carbamate species.[33] Simultaneously, the bands at 1469 and 1386 cm^{-1} are due to the $\nu(CO_3^{2-})$ asymmetrical modes of polydentate carbonate species adsorbed on ceria and the 1292 cm^{-1} band assigned to bidentate carbonate species (Figure 11b).[34] At the same time, O-H stretching modes of terminal (t-OH) and bridged (b-OH) hydroxyl groups (bands at 3729 and 3626 cm^{-1}) were observed and the bands at 3706 and 3599 cm^{-1} were due to the combination of Fermi resonance doublet at 1386 and 1292 cm^{-1} of adsorbed CO_2 with the fundamental at 233 cm^{-1} (trapped CO_2).[35] Over the MnO_x(0.03)-CeO_2 catalyst, the adsorption form of BA were similar with that of Lab-CeO_2 catalyst. However, after introduction of CO_2, only the band at 1651 cm^{-1} characteristic of carbonyl stretching vibrations of carbamic acid or carbamate was obviously observed but no bidentate and polydentate carbonate species were observed. These results showed that although CO_2 reacted with BA to carbamate or carbamic acid over the Lab-CeO_2 catalyst at 170 ^oC, CO_2 can adsorb on the catalyst surface to form less active but stable bidentate and

polydentate carbonate species. However, MnO_x(0.03)-CeO_2 catalyst not only favored the formation of carbamate or carbamic acid but also inhibited the further formation of stable bidentate and polydentate carbonate species under ambient CO_2 atmosphere.

<Please insert Figure 11 here>

Then, CH_3OH was introduced in CO_2 flow to the Lab-CeO_2 and MnO_x (0.03)-CeO_2 catalyst at reaction temperature 170 ^oC (Figure 12). Over the Lab-CeO_2 catalyst, after the introduction of methanol for 5 min, the undissociated adsorbed methanol species occurred (the ν_{CO} modes at ca. 1055 cm^{-1} and 1032 cm^{-1}).[36] Most importantly, dissociated adsorption of methanol happened at the same time. The monodentate species (type I, 1102 cm^{-1}), bidentate species on Ce^{4+} (type II', 1049 cm^{-1}) and triply bridging methoxy species (type III, 1014 cm^{-1}) can be observed as well as the C–H stretching bands (2820, 2843, and 2922 cm^{-1}) and $\delta(CH_3)$ deformation mode band 1454 cm^{-1} (Scheme 3).[37] Simultaneously, new peaks 1478, 1346, 1303, and 1209 cm^{-1} characteristic of methyl carbonates-like species occurred with the retaining carbamate or carbamic species (1652 cm^{-1}), demonstrating that CO_2-derivated species including the carbamate species react with methoxy adspecies of methanol to obtain methyl carbonates-like species and all these species co-existed on the catalyst surface.[38] When the time was prolonged to 15 min, the bidentate species on Ce^{3+} (type II, 1059 cm^{-1}) began to come up and then the species type II* (transformed from type I, 1063 cm^{-1}) appeared after 20 min. Similarly, over the MnO_x(0.03)-CeO_2 catalyst, type I (1102 cm^{-1}), type II* (1063 cm^{-1}), type II (1057 cm^{-1}) and type II' (1051 cm^{-1}) methoxy species as well as the formed methyl carbonates-like species were all observed after the addition of methanol for 30 min. However, the band resulted from methoxy adspecies of type III (1014 cm^{-1}), which was less active to react with CO_2-derivated species, was very weak so that almost cannot be observed. Whereupon, we can find that the MnO_x(0.03)-CeO_2 catalyst favored the formation of type I, type II and type II' species and inhibited the formation of the non-reactive type III species thereby promoting the removing of the carbonaceous species.

<Please insert Figure 12 here>

<Please insert Scheme 3 here>

Notably, over Lab-CeO_2 catalyst, the adsorbed species generated from CO_2, BA and methanol were largely reduced when the temperature was increased to 300 ^oC and almost disappeared at 500 ^oC (Figure 13). The bands 3729 and 3626 cm^{-1} assignable to the O-H stretching disappeared at 300 ^oC and a new broad peak at 3399 cm^{-1} appeared which was due to OH species adsorbed on reduced ceria, arisen from Ce^{4+}-Ce^{3+} redox in the reaction. Nevertheless, no peak at 3399 cm^{-1} can be observed over MnO_x(0.03)-CeO_2 catalyst, which offered another evidence that the surface-subsurface reorganization of the Lab-CeO_2 happened more easily, in comparison with that of MnO_x(0.03)-CeO_2 catalyst.[34,39]

<Please insert Figure 13 here>

Conclusion

The deactivation mechanism of the CeO_2-based catalysts and also the role of Mn doping in MnO_x (0.03)-CeO_2 catalyst on enhancing the recyclability of the catalyst have been investigated by catalytic activity tests, reaction kinetics and characterization techniques (XRD, Raman, TG, CO_2-TPD, XPS, and DRIFT studies). It was demonstrated that a certain amount of the carbonate-like species arisen from the catalytic reaction covered the surface of CeO_2 catalysts, which induced a surface reorganization, mainly contributing to the deactivation of Lab-CeO_2 or CeO_2 catalyst. However, the Mn doping in the MnO_x (0.03)-CeO_2 catalyst can weaken the interaction with the CO_2 and promote the dissociative adsorption of the methanol, allowing the dissociated species to react with the carbonaceous species on the surface of the catalyst, resulting in more stable surface structure and thus enhancing the recyclability of the catalyst. In summary, we have developed new heterogeneous and recyclable CeO_2-based catalysts for CO_2 conversion, which provides an approach for the design of efficient catalyst used for the catalytic synthesis of carbamate from carbon dioxide.

Acknowledgements

The authors are grateful for support from the National Natural Science Foundation of China (21373082), innovation Program of Shanghai Municipal Education Commission (15ZZ031), and the Fundamental Research Funds for the Central Universities.

Reference

1 *Urethane protecting groups* in *Protective Groups in Organic Synthesis*, 4th edn, ed. P. G. M. Wuts and T. W. Greene, J. Wiley & Sons, 2006.

2 O. Kreye, H. Mutlu and M. A. R. Meier, *Green Chem.*, 2013, **15**, 1431.

3 (a) *Ullmann's Encyclopedia of Industrial Chemistry*, 6th edn, ed. A. Eckerle, Wiley VCH Germany, Weinheim, 2000; (b) H. Eckert and B. Foster, *Angew. Chem., Int. Ed.*, 1987, **26**, 894.

4 M. E. Boot-Handford, J. C. Abanades, E. J. Anthony, M. J. Blunt, S. Brandani, N. M. Dowell, J. R. Fernández, M. C. Ferrari, R. Gross, J. P. Hallett, R. S. Haszeldine, P. Heptonstall, A. Lyngfelt, Z. Makuch, E. Mangano, R. T. J. Porter, M. Pourkashanian, G. T. Rochelle, N. Shah, J. G. Yao and P. S. Fennell., *Energy Environ. Sci.*, 2014, **7**, 130.

5 M. Gasperini, F. Ragaini, S. Cenini and E. *Gallo, J. Mol. Catal. A: Chem.*, 2003, **204-205**, 107.

6 B. Chen and S. S. C. Chuang, *Green Chem.*, 2003, **5**, 484.

7 J. J. Gao, H. Q. Li, Y. F. Zhang and Y. Zhang, *Green Chem.*, 2007, **9**, 572.

8 (a) T. Baba, A. Kobayashi, Y. Kawanami, K. Inazu, A. Ishikawa, T. Echizenn, K. Murai, S. Aso and M. Inomata, *Green Chem.*, 2005, **7**, 159; (b) M. Selva, P. Tundo, A. Perosa and F. Dall'Acqua, *J. Org. Chem.*, 2005, **70**, 2771.

9 (a) M. Aresta, A. Dibenedetto and A. Angelini, *Chem. Rev.*, 2014, **114**, 1709; (b) T. Sakakura, J. C. Choi and H. Yasuda, *Chem. Rev.*, 2007, **107**, 2365.

10 M. Mikkelsen, M. Jørgensen and F. C. Krebs, *Energy Environ. Sci.*, 2010, **3**, 43.

11 (a) A. Dibenedetto, A. Angelini and P. Stufano, *J. Chem. Technol. Biotechnol.*, 2014, **89**, 334; (b) M. Aresta and A. Dibenedetto, *Dalton Trans.*, 2007, 2975; (c) S. N. Riduan and Y. Zhang, *Dalton Trans.*, 2010, **39**, 3347.

12 D. Chaturvedi, *Tetrahedron*, 2012, **68**, 15.

13 (a) M. Abla, J. C. Choi and T. Sakakura, *Chem. Commun.*, 2001, 2238; (b) M. Abla, J. C. Choi and T. Sakakura, *Green Chem.*, 2004, **6**, 524; (c) A. Ion, C. V. Doorslaer, V. Parvulescu, P. Jacobs and D. D. Vos, *Green Chem.*, 2008, **10**, 111.

14 M. Honda, S. Sonehara, H. Yasuda, Y. Nakagawa and K. Tomishige, *Green Chem.*, 2011, **13**, 3406.

15 (a) R. Zhang, L. Hua, L. Guo, B. N. Song, J. Z. Chen and Z. S. Hou, *Chin. J. Chem.*, 2013, **31**, 381; (b) R. Zhang, L. Guo, J. Z. Chen, H. M. Gan, B. N. Song, W. W. Zhu, L. Hua, and Z. S. Hou, *ACS Sustainable Chem. Eng.*, 2014, **2**, 1147.

16 Z. Wang, G. l. Shen, J. Q. Li, H. D. Liu, Q. Wang and Y. F. Chen, *Appl. Catal., B: Environ.*, 2013, **138-139**, 253.

17 A. E. Nelson and K. H. Schulz, *Appl. Surf. Sci.*, 2003, **210**, 206.

18 N. M. Marta, B. Giovanni and G. Antonella, *Chem. Mater.*, 2005, **17**, 6272.

19 B. Fazio, L. Spadaro, G. Trunfio, J. Negro and F. Arena, *J. Raman Spectrosc.*, 2011, **42**, 1583.

20 F. Arena, G. Trunfio, B. Fazio, J. Negro and L. Spadaro, *J. Phys. Chem. C*, 2009, **113**, 2822.

21 J. M. López, R. Arenal, B. Puértolas, Á. Mayoral, S. H. Taylor, B. Solsona and T. García, *J. Catal.*, 2014, **317**, 167.

22 A. Primo, E. Aguado, and H. Garcia, *ChemCatChem*, 2013, **5**, 1020.

23 M. C. Ribeiro, G. Jacobs, B. H. Davis, L. V. Mattos and F. B. Noronha, *Top. Catal.*, 2013, **56**, 1634.

24 F. Larachi, J. Pierre, A. Adnot and A. Bernis, *Appl. Surf. Sci.*, 2002, **195**, 236.

25 G. Z. Chen, F. Rosei and D. L. Ma, *Adv. Funct. Mater.*, 2012, **22**, 3914.

26 D. Wolf, M. Heber, W. Grünert and M. Muhler, *J. Catal.*, 2001, **199**, 92.

27 (a) X. Y. Wang, Q. Kang and D. Li, *Appl. Catal., B: Environ.*, 2009, **86**, 166; (b) H. C. Yao and Y. F. Yu Yao, *J. Catal.*, 1984, **86**, 254.

28 F. Arena, G. Trunfio, J. Negro, B. Fazio, and L. Spadaro, *Chem. Mater.*, 2007, **19**, 2269.

29 (a) C. H. Kim and L. T. Thompson, *J. Catal.*, 2005, **230**, 66; (b) A. Bumajdad, M. I. Zaki, J. Eastoe and L. Pasupulety, *Langmuir*, 2004, **20**, 11223; (c) A. Karpenko, R. Leppelt, J. Cai, V. Plzak, A. Chuvilin, U. Kaiser and R. J. Behm, *J. Catal.*, 2007, **250**, 139.

30 (a) L. G. Appel, J. G. Eon and M. Schmal, *Catal. Lett.*, 1998, **56**, 199; (b) H. S.

Roh, A. Platon, Y. Wang and D. L. King, *Catal. Lett.*, 2006, **110**, 1.

31 (a) *X-Ray Photoelectron Spectroscopy of Solid Surfaces*, ed. V. I. Nefedov, first English ed., VSP, Utrecht, 1988; (b) *Hand book of monochromatic XPS spectra: The Elements and Native oxides*, ed. B. V. Crist, XPS International, Ames. Iowa, John Wiley & Sons, LTD, Weinheim, 1999; (c) *High resolution XPS of organic polymers: The Scienta ESCA 300 Database*, ed, G. Beamson and D. Briggs, John Wiley & Sons, LTD, Weinheim, 1992.

32 M. Tamura, T. Tonomura, K. Shimizu, and A. Satsuma, *Green Chem.*, 2012, **14**, 717.

33 M. Tamura, M. Honda, K. Noro, Y. Nakafawa, K. Tomishige, *J. Catal.*, 2013, **305**, 191.

34 E. Finocchio, M. Daturi, C. Binet, J. C. Lavalley, *Catalysis Today*, 1999, **52**, 53.

35 (a) Y. Ikeda, M. Asadullah, K. Fujimoto, and K. Tomishige, *J. Phys. Chem. B*, 2001, **105**, 10653; (b) E. Finocchio, and G. Busca, *Catalysis Today*, 2001, **70**, 213.

36 R. Juárez, P. Concepción, A. Corma and H. García, *Chem, Commun.*, 2010, **46**, 4181.

37 (a) M. Tamura, A. Satsuma and K. Shimizu, *Catal. Sci. Technol.*, 2013, **3**, 1386; (b) A. Badri, C. Binet and J. C. Lavalley, *J. Chem. Soc., Faraday Trans.*, 1997, **93**, 1159.

38 (a) C. Binet, M. Daturi and J. C. Lavalley, *Catal. Today*, 1999, **50**, 207; (b) J. Lamotte, V. Morávek, M. Bensitel and J. C. Lavalley, *React. Kinet. Catal. Lett.*, 1988, **1**, 113-118.

39 H.Tsuji, A. O. Yoshida, T. Shishido, and H. Hattori, *Langmuir*, 2003, **19**, 8793.

Scheme 1 Carbamate synthesis from BA, CO_2 and methanol.

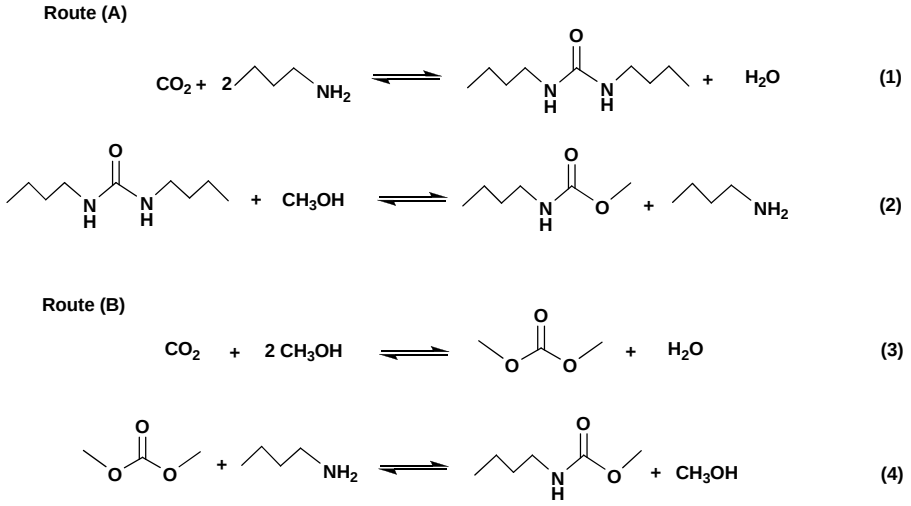

Scheme 2 Possible reaction routes in carbamate synthesis.

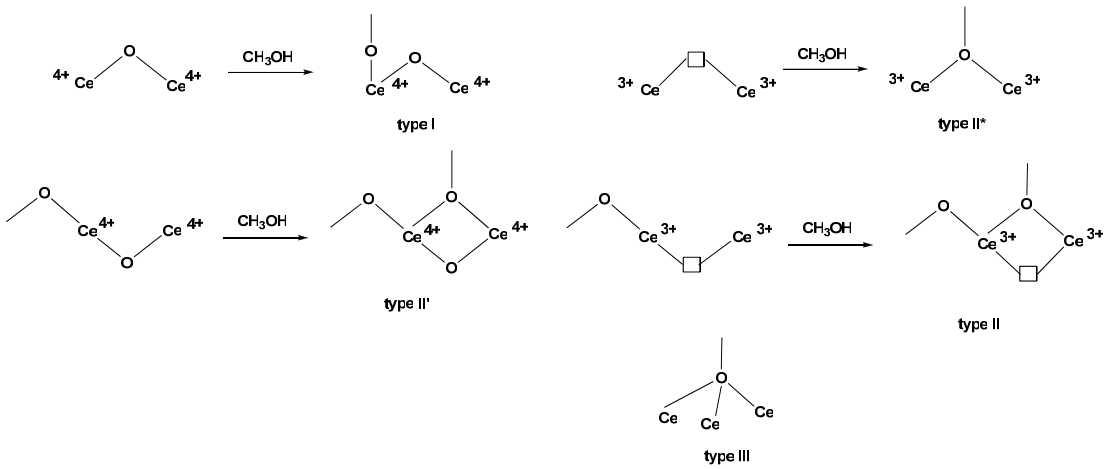

Scheme 3 The adspecies of methanol over Lab-CeO_2 and MnO_x (0.03)-CeO_2 catalysts.

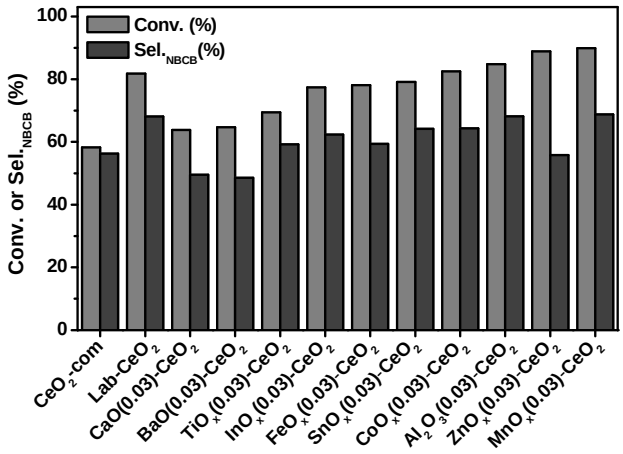

Figure 1 Carbamate synthesis over the different catalysts. Reaction condition: BA: CH_3OH = 5 mmol: 200 mmol, t = 16 h, T = 170 ^oC, P = 5.0 MPa, catalyst 0.3 g. The main by-products were N-methylbutylamine and dibutylurea. Conversion of BA (%) = (Moles of BA consumed/Moles of BA used in the reaction) ×100; selectivity to NBNB (%) = (Moles of NBNB/Moles of BA reacted) ×100. The conversion and selectivity in other tables and figures were obtained by the similar method.

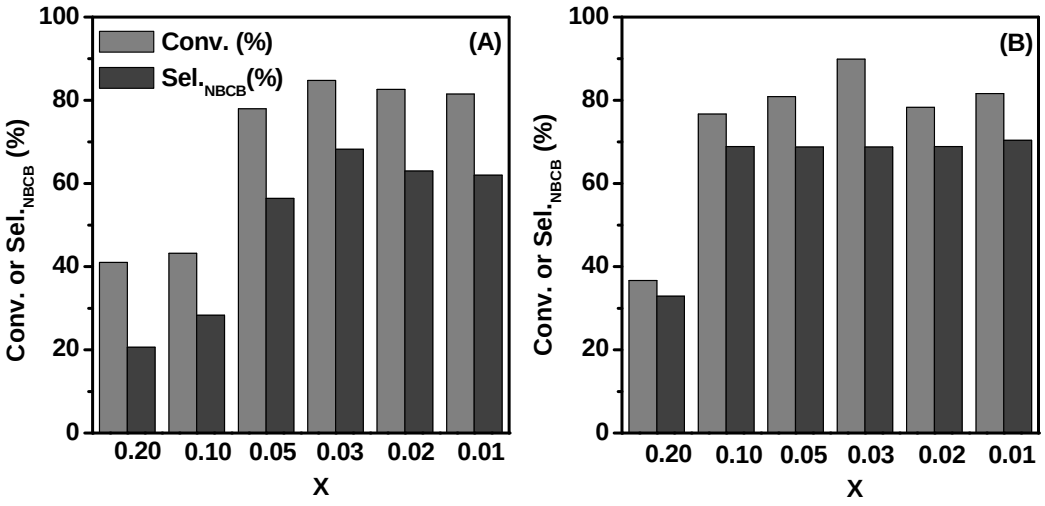

Figure 2 Effect of catalyst composition (Al_2O_3(X)-CeO_2 and MnO_x(X)-CeO_2) on the conversion of BA and selectivity to NBCB. Reaction condition: BA: CH_3OH = 5 mmol: 200 mmol, t = 16 h, T = 170 ^oC, P = 5.0 MPa, catalyst 0.3 g.

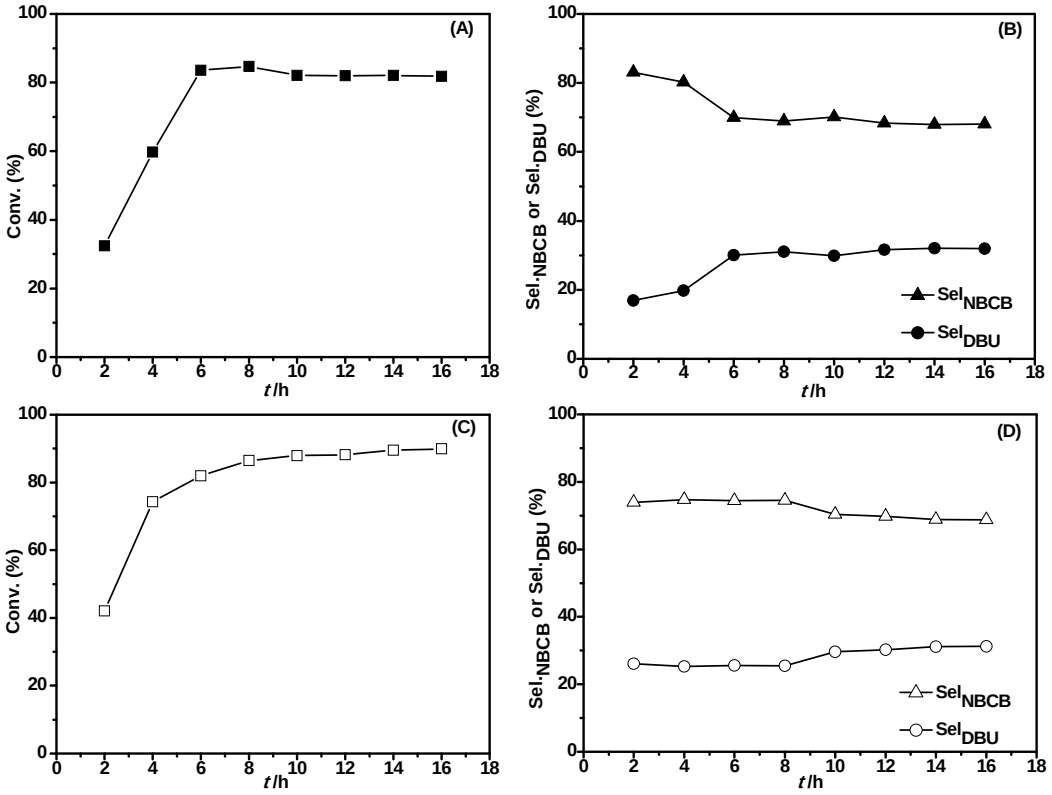

Figure 3 The conversion of BA and selectivity to NBCB and DBU versus time profile over Lab-CeO_2 catalyst (top A and B) and MnO_x(0.03)-CeO_2 catalyst (bottom C and D). Reaction condition: BA: CH_3OH=5 mmol: 200 mmol, T = 170 ^oC, P = 5.0 MPa, catalyst 0.3 g.

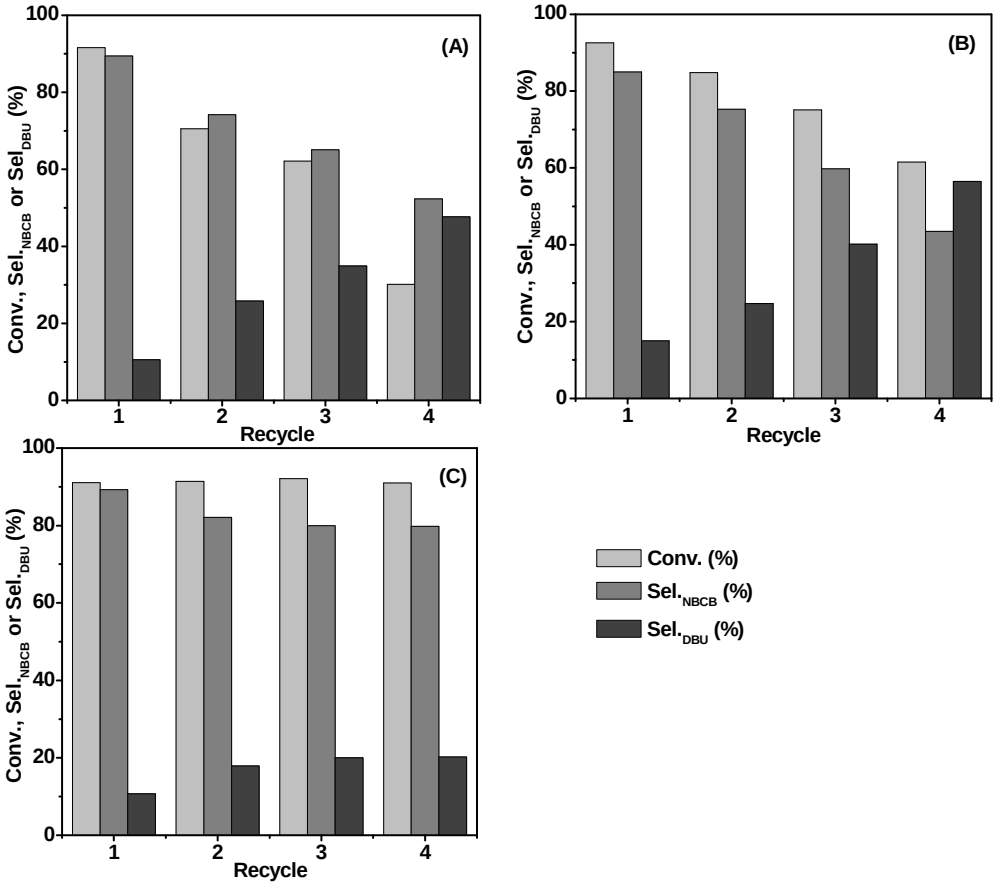

Figure 4 Recyclability of (A) Lab-CeO_2, (B) Al_2O_3 (0.03)-CeO_2 and (C) MnO_x (0.03)-CeO_2 catalyst. Reaction condition: BA: CH_3OH = 5 mmol: 500 mmol, t = 8 h, T = 170 ^oC, P = 5 MPa, catalyst 0.3 g.

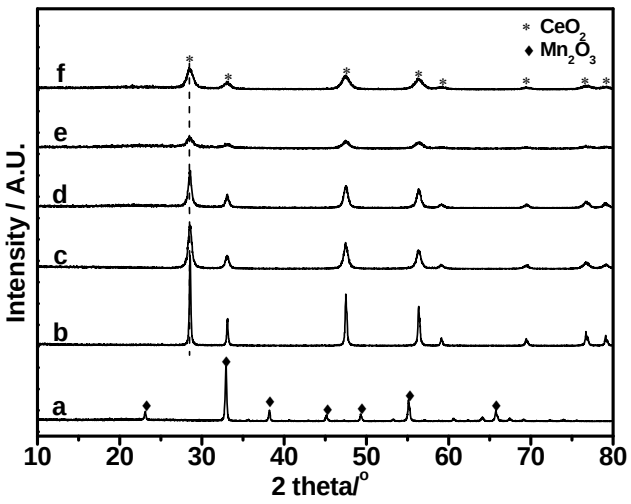

Figure 5 XRD patterns of different catalysts. (a) Mn_2O_3, (b) CeO_2-com, (c) Lab-CeO_2, (d) the spent Lab-CeO_2, (e) MnO_x(0.03)-CeO_2, and (f) the spent MnO_x(0.03)-CeO_2.

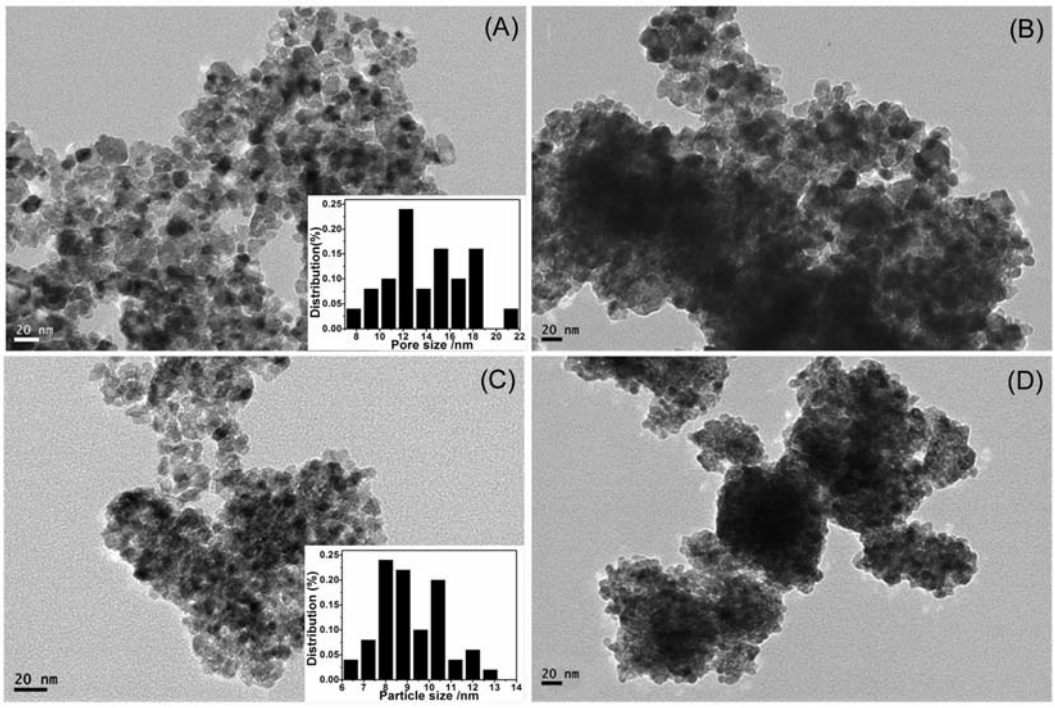

Figure 6 TEM images of different catalyst. (A) Lab-CeO_2, (B) the spent Lab-CeO_2, (C) MnO_x(0.03)-CeO_2, and (D) the spent MnO_x(0.03)-CeO_2.

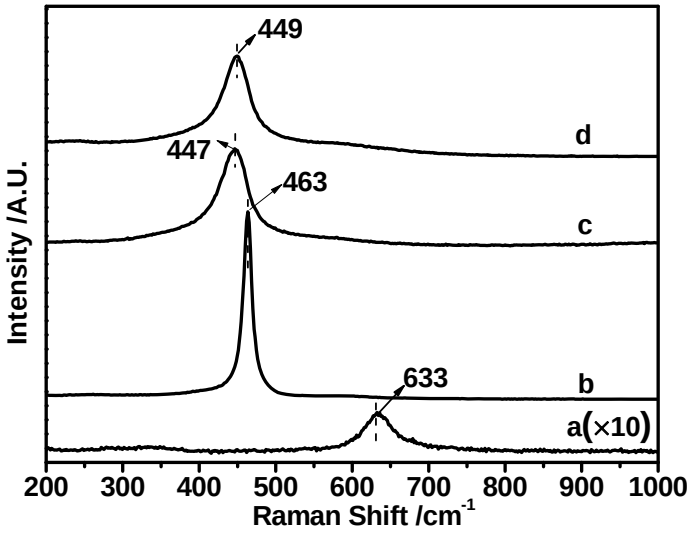

Figure 7 Raman spectra from 200 to 1000 cm^{-1} of the Lab-CeO_2 and MnO_x (0.03)-CeO_2 catalysts. (a) Mn_2O_3, (b) Lab-CeO_2, (c) MnO_x(0.03)-CeO_2, and (d) the spent MnO_x(0.03)-CeO_2.

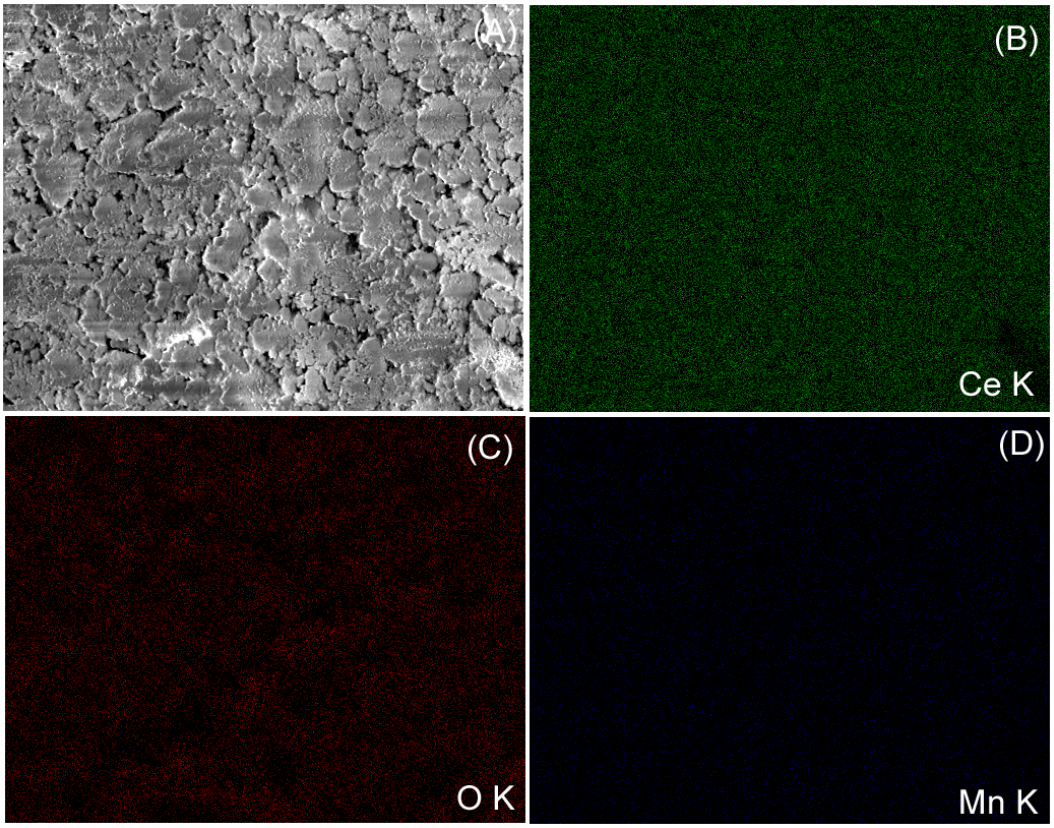

Figure 8 SEM-EDS analysis of the $MnO_x(0.03)$-CeO_2 catalyst: SEM image of the catalyst (A), and corresponding X-ray maps of Ce (B), O (C), and Mn (D).

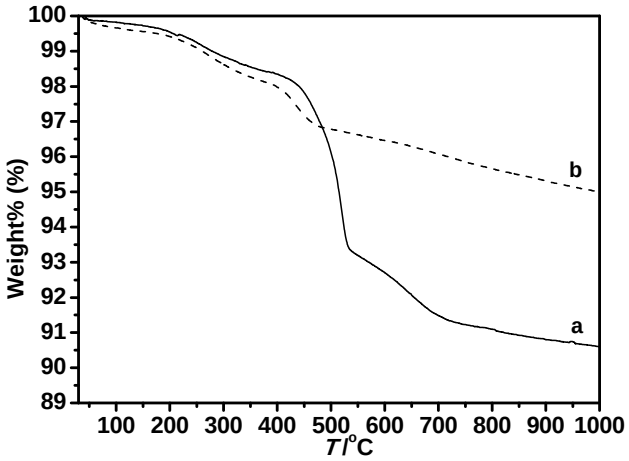

Figure 9 TG profiles of the catalysts. (a) the spent Lab-CeO_2 catalyst (b) the spent MnO_x(0.03)-CeO_2 catalyst.

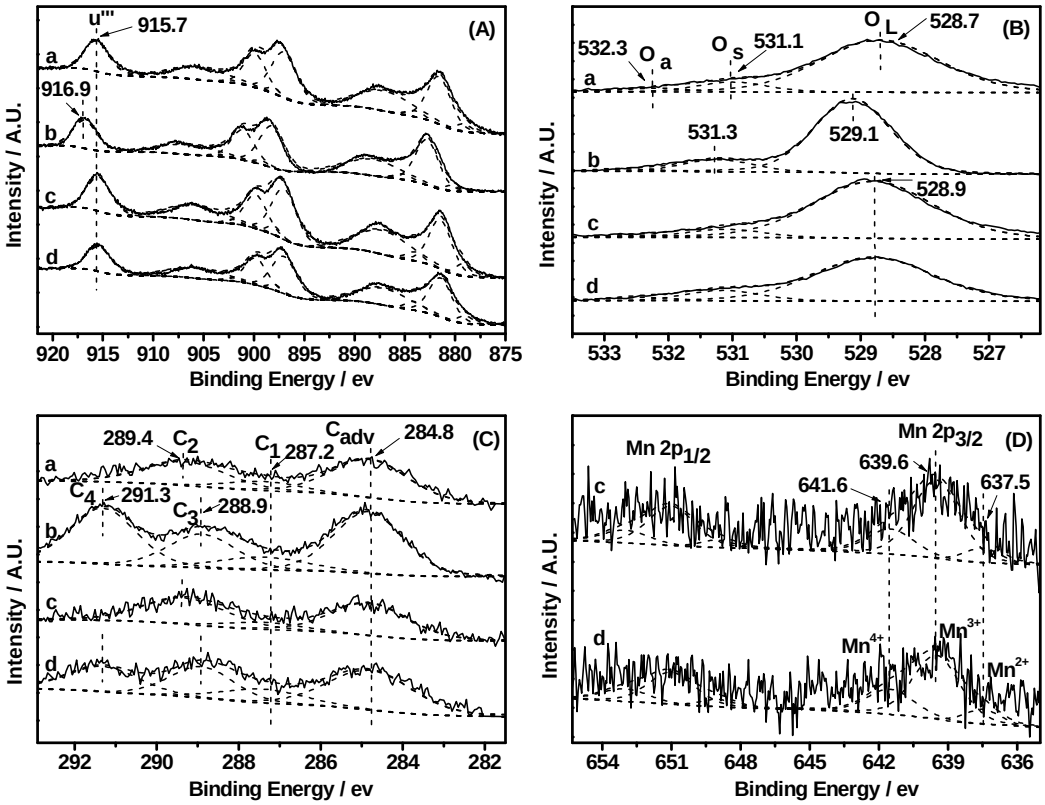

Figure 10 Deconvoluted XPS peaks monitored over the Ce 3d (A), O 1s (B), C 1s (C) and Mn 2p (D) photoelectron emission regions for the (a) Lab-CeO_2, (b) the spent Lab-CeO_2, (c) MnO_x (0.03)-CeO_2, and (d) the spent MnO_x (0.03)-CeO_2.

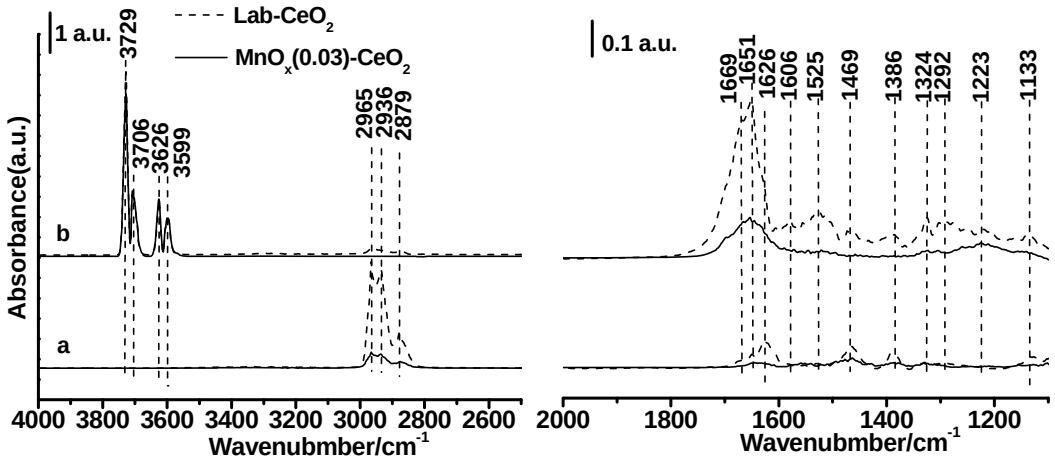

Figure 11 DRIFT spectra of *in-situ* BA adsorbed on Lab-CeO_2 (dashed lines) and MnO_x (0.03)-CeO_2 catalyst (solid lines) at He flow at 170 ^oC (a), and introduction of CO_2 to BA adsorbed catalysts (b).

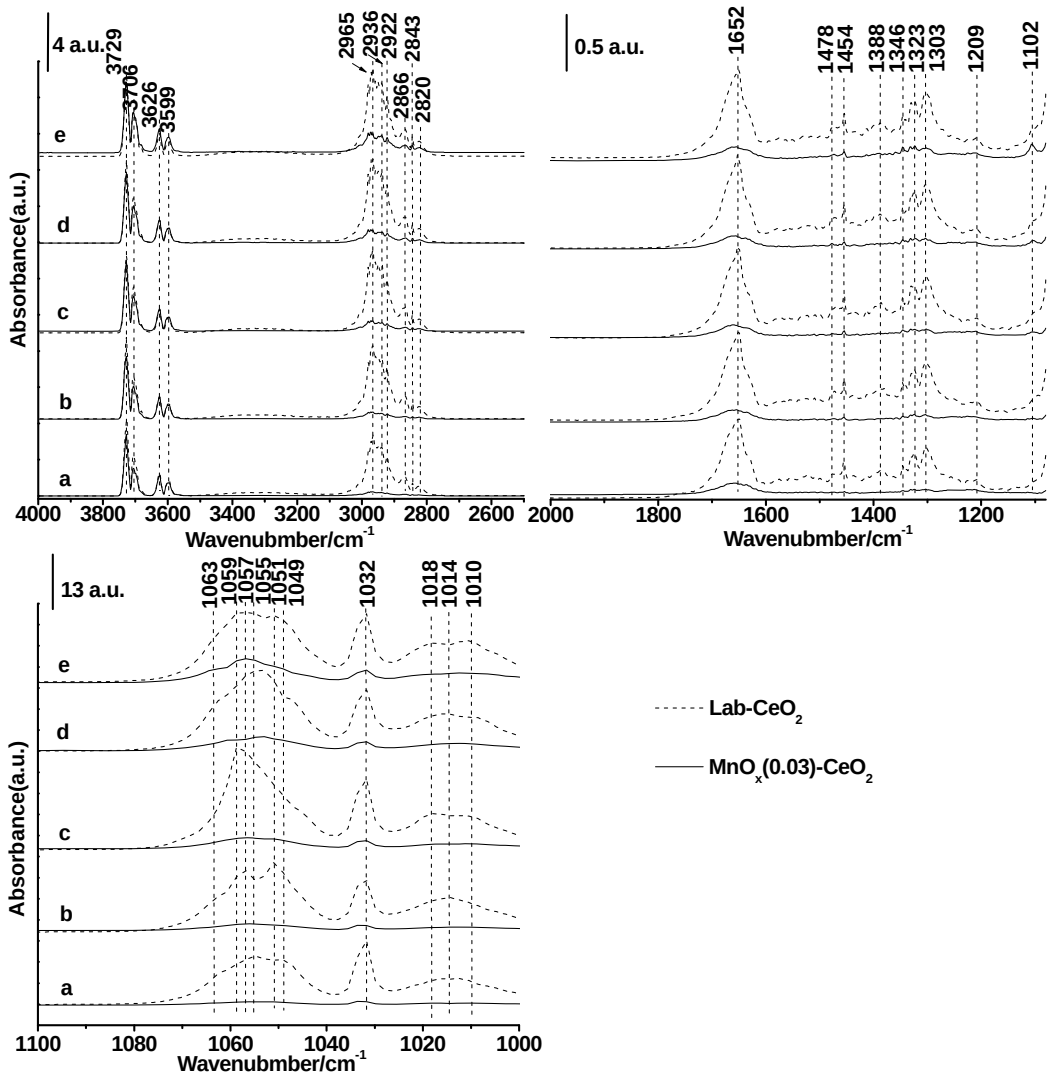

Figure 12 DRIFT spectra of *in-situ* co-absorbed methanol on the BA and CO_2 adsorbed Lab-CeO_2 (dashed lines) and MnO_x(0.03)-CeO_2 catalyst (solid lines) at 170 ^oC recorded after the methanol was introduced for 5 min (a), 10 min (b), 15 min (c), 20 min (d), and 30 min (e).

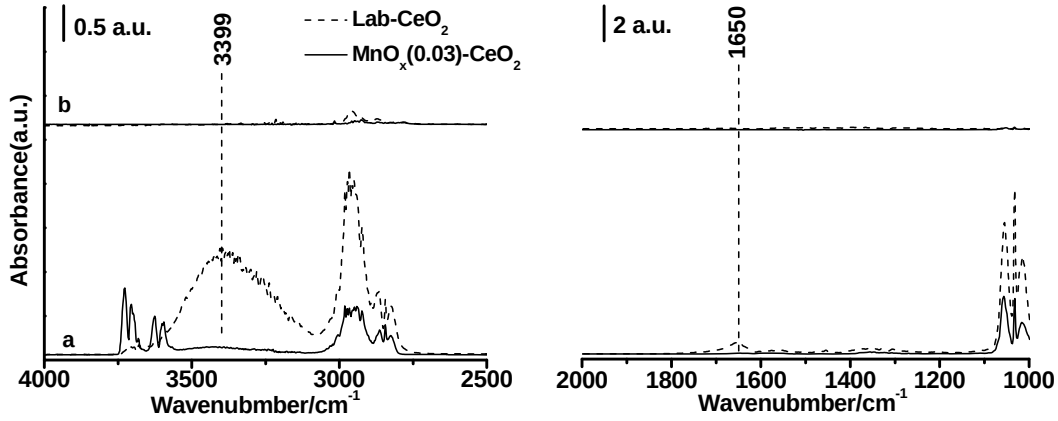

Figure 13 FT-IR spectra of BA, CO_2 and CH_3OH co-adsorbed Lab-CeO_2 (dashed lines) and MnO_x (0.03)-CeO_2 catalyst (solid lines) recorded after heating up to 300 ^oC for 5 min (a) and 500 ^oC for 15 min (b) in He flow.

Table 1 Carbonylation of BA with CO_2 using CeO_2 and MnO_x (0.03)-CeO_2 catalysts[a]

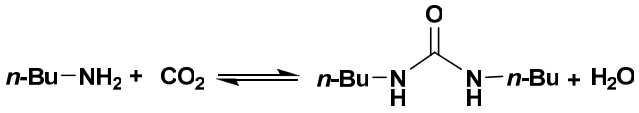

Entry	Catalyst	/%	$Sel._{DBU}$/%
1	Lab-CeO_2	48.9	100
2	2nd run	33.8	100
3	3rd run	None	None
4	MnO_x (0.03)-CeO_2	51.8	100
5	2nd run	50.4	100
6	3rd run	54.7	100

[a]Reaction condition: BA = 5 mmol, T = 170 °C, P = 5.0 MPa, t = 8 h, catalyst 0.3 g.

Table 2 Alcoholysis of DBU to NBCB catalyzed by Lab-CeO_2 and MnO_x (0.03)-CeO_2 under the pressure of N_2 or CO_2.[a]

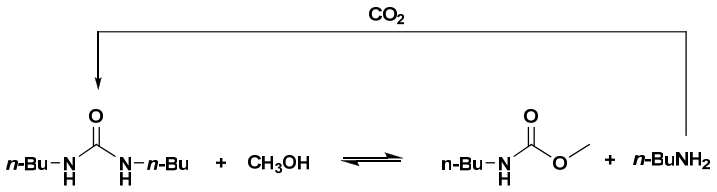

Entry	Catalyst	Atmosphere	Product after the reaction /mmol			
			n_{NBCB}	n_{BA}	n_{DBU}	n_{DMC}
1	none	N_2	1.0	1.1	1.4	none
2	Lab-CeO_2	N_2	1.8	2.0	0.6	none
3	2nd run	N_2	1.9	1.7	0.7	none
4	Lab-CeO_2	CO_2	2.7	0.5	0.8	0.2
5	2nd run	CO_2	2.0	0.6	1.2	0.4
[b]6	3rd run	CO_2	1.2(2.9)	1.0(0.5)	1.4(0.8)	0.5(0.6)
7	MnO_x(0.03)-CeO_2	CO_2	3.8	0	0.6	0.8
8	2nd run	CO_2	4.0	0	0.5	0.5
9	3rd run	CO_2	3.9	0	0.5	0.9

[a]Reaction condition: DBU = 2.5 mmol, CH_3OH = 500 mmol, T = 170 ^oC, P = 5.0 MPa, t = 8 h, catalyst 0.3 g. [b]The product mmoles in the parenthesis refers to that for the third run after the spent catalyst was calcined in O_2 at 220 ^oC for 2 h prior to use.